PHYSICAL REVIEW B VOLUME 6, NUMBER 10 15 NOVEMBER 1972

Tunneling Spectroscopy and Band-Structure Effects in *n* GaSb under Pressure*

P. Guétin† and G. Schréder
Laboratoires d'Electronique et de Physique Appliquée, 94-Limeil-Brévannes, France
(Received 18 May 1972)

The effect of hydrostatic pressure (up to 16 kbar) on the characteristics of n-type-GaSb–Pb tunnel contacts has been investigated both experimentally and theoretically. The background resistance dV/dI exhibits huge changes when the ⟨000⟩- and ⟨111⟩-conduction-band extrema cross each other. In the indirect-gap configuration, the tunnel current results from four contributions: (i) the specular component corresponding to the ⟨111⟩ valleys, (ii) beyond a negative threshold voltage, an additional specular part related to the ⟨000⟩ minimum which leads to a direct measurement of the interband energy gap, (iii) a phonon-assisted current which provides the first determination of zone-edge phonon energies in the ⟨111⟩ directions, and (iv) an impurity-assisted mechanism. Application of pressure in GaSb constitutes an original way of continuously varying the Fermi degeneracy. This has some striking influence on the line shape, parity, magnitude, and position of phonon structures displayed by the tunneling characteristics.

I. INTRODUCTION

Tunneling in solids has often been studied for the purpose of obtaining information about the band structure of the materials which constitute the junctions.[1,2] In many instances, detailed features of the band structure are only weakly displayed in the tunneling characteristics. However, large band-structure effects can be observed in some special cases. For example, it is possible to detect a dramatic bias-induced onset of tunneling into a higher band in indirect-gap materials. This effect occurs in reverse-biased n-Ge tunnel contacts.[3] Another spectacular band-structure effect in indirect-gap materials is the phonon-assisted tunneling mechanism first observed in n Ge.[4,5] At present, it appears that these large band-structure effects (upper-valley-electron states and phonon-assisted tunneling) occur only in indirect-gap semiconductors. Therefore, external means of controlling the band structure and thereby affecting the tunneling characteristics appear very attractive. To this end, we investigated metal-GaSb contacts under hydrostatic pressure.[6]

GaSb is a direct-gap semiconductor at atmospheric pressure. The ⟨111⟩ valleys lie at an energy $\Delta E \simeq 85$ meV above the bottom ⟨000⟩ of the conduction band at 4.2 °K. The experimental values are generally scattered between 78 and 95 meV.[7–15] A typical characteristic of the measurements is either the inaccuracy of the method or the indirect way in which ΔE is extracted from the experimental data. The main difficulties result from the nonparabolicity of the conduction band and the uncertainties in other parameters such as effective masses and mobilities. Hydrostatic pressure induces a shift of both conduction-band minima away from the valence-band maximum towards higher energy (Fig. 1). The rate of change of their energy difference $(\partial/\partial P)(E_L - E_\Gamma)$ has been found to be[16] -9.6 meV/kbar, and the gap becomes indirect around $P_0 = 9$ kbar. We have shown in a preliminary report[6] that the tunnel characteristics are reasonably "n-GaAs-like" below P_0 and "n-Ge-like" at higher pressures. Because the effective mass $m_\Gamma^* < m_L^*$, two unambiguous band-structure effects occur above P_0: the appearance of a zone-edge phonon-assisted current and the onset of tunneling into the higher valley at reverse bias. The former constitutes the first experimental determination of the zone-edge phonon energies in the ⟨111⟩ direction; the latter is the most *direct* method of measurement of the interband energy gap which has been used to date.

Since we have undertaken a new set of experiments below 9.6 kbar (the low-pressure limit of our previous measurements[6]), this paper offers a complete survey of the tunnel effect in GaSb Schottky barriers from 0 to 16 kbar. We also report an experimental study of the barrier-height variation between 0 and 15 kbar. This allows us to compare our results with a theory predicting the shape and magnitude of the differential resistance at any pressure. We conclude that ΔE is somewhat higher than expected and is slightly dependent on the carrier density. It is also likely that an additional nonspecular tunnel current appears when the gap is indirect. The application of pressure constitutes an unique way of continuously varying the Fermi degeneracy and the carrier density in the Γ band. This influences the line shape, parity, amplitude, and position of phonon and plasmon structures contained in the tunneling characteristics. Our results, therefore, add significant details to the understanding of the effects of electron-phonon interactions in the barrier and in the semiconductor electrode.

Section II contains the experimental details.

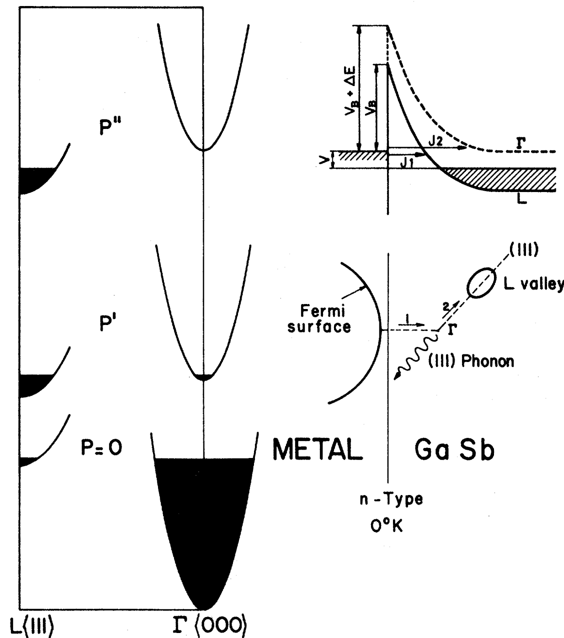

FIG. 1. Three pressure-dependent positions of the conduction-band minima in GaSb (on the left) and the two expected main phenomena: the onset of tunneling into the central valley at reverse bias (upper right) and the appearance of a zone-edge phonon-assisted current.

Section III is devoted to the results of the tunnel effect at atmospheric pressure and Sec. IV contains the high-pressure experimental results and analysis. Section V is a discussion of our major results and Sec. VI contains some possible applications to the study of the band structure of semiconductors.

II. EXPERIMENTAL METHODS

A. Junction Preparation and Sample Holder

Tunnel contacts were made in an ultra-high vacuum system by cleaving a ⟨110⟩ bar of n GaSb : Te

TABLE I. Cleaved n-GaSb–Pb (CGSP) contacts: samples' characteristics.

Sample (CGSP)	Doping density N (cm^{-3})	Type of experiments
11	(300 °K) 3×10^{17}	Barrier height at $P=0$
13	2.5×10^{17}	
10	3.5×10^{17}	Barrier height at $P=0$
14	3.5×10^{17}	and up to 15 kbar
5	(4.2 °K) 1.3×10^{18}	Tunneling at $P=0$
8	3.35×10^{18}	
7	3.5×10^{18}	Tunneling between 0 and 12 kbar
1	3.75×10^{18}	Tunneling between 10 and 16 kbar

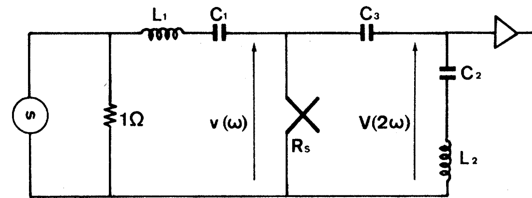

FIG. 2. Second-derivative network.

in the stream of the evaporating metal (lead).[17] Three to five metal dots located on an area free of cleavage steps were selected as the samples listed in Table I. Hall measurements using a cloverleaf geometry were carried out on slices adjacent to the tunnel or capacitance samples (see Appendix A). Minor differences in N, the carrier density, of samples numbered CGSP 1, 7, and 8 resulted from cleaving different regions of the same GaSb ingot containing a slight doping gradient. At least three samples are required to cover the entire experimental range because of the great increase of the tunnel resistance under pressure. The pressure experiments were carried out at the Faculté des Sciences d'Orsay.[17,18] The measurements were done at 4.2 °K and up to 16 kbar with no applied magnetic field. Atmospheric-pressure studies were performed down to 0.9 °K by pumping on the helium bath; a magnetic field could be applied to quench the superconductivity in the metal. The quality of the tunnel contacts was checked by observing the superconducting density of states at each pressure sitting.

B. Measuring System

The barrier height has been measured by the differential-capacitance method. The tunnel-current first and second derivatives were obtained by a classical modulation technique using a lock-in-amplifier system.[19] The electronic circuit is such that the second-harmonic voltage $V(2\omega)$ is not generally proportional to d^2I/dV^2. This feature is of some importance when we want to compare experiment with theory or simply calculate the magnitude of a structure. Indeed, referring to Fig. 2, a constant voltage of frequency $\omega = 517$ Hz appears across the 1-Ω input to the reactive circuit. The L_1C_1 circuit is tuned to ω and rejects the unwanted second-harmonic voltage coming from the oscillator. It also prevents the signal at 2ω generated by the junction of dynamic resistance R_s to be shunted by the 1-Ω resistance. Beyond the junction, the L_2C_2 circuit is tuned to ω and the $L_2C_2C_3$ circuit to 2ω. As a result, the output mesh simultaneously feeds the harmonic voltage to the input of the high-gain preamplifier and provides a suppression of the fundamental signal. It

can be easily shown that

$$V(2\omega)=\frac{3R_s i'' e^2 L_2\omega}{8(R_s+R_{L_2})}\cos 2\omega t\ , \qquad (1)$$

where R_{L_2} is the resistance of the inductance L_2 and e is the amplitude of the fundamental signal. The primary objective of the second-derivative method is to obtain the general shape of the i''-vs-V curve (i'' is the true d^2I/dV^2 and V the bias voltage) and to determine the exact line shape of the spectroscopic structures. The electronic system directly provides i'' only when $R_s \gg R_{L_2}$. Indeed, R_s falls out of Eq. (1) and e keeps a constant value as R_s varies. For example, this is the case for sample CGSP 5 whose zero-bias resistance ranges from 500 to 900 Ω, whereas R_{L_2} is equal to 19 Ω at 1 kHz. When the junction has a smaller resistance, an appropriate correction must be made in order to recover i'' from the experimental $V(2\omega)$.

Another aspect of the second-derivative method is to provide a measurement of the relative conductance variation $d\sigma/\sigma$, of the fine structures. Since we have

$$\frac{d\sigma}{\sigma}=\int R_s\, i''\, dV\ , \qquad (2)$$

$R_s i''$ must be considered as a complete entity in Eq. (1) and we take advantage of lowering the quantity $R_s+R_{L_2}$. In fact, the weakness of some structures imposes generally to work in the optimal noise conditions. This implies that we must choose low resistive samples with $R_s \simeq R_{L_2}$. $d\sigma/\sigma$ can be easily evaluated from Eqs. (1) and (2) by measuring the area of the curve $V(2\omega)$ obtained from the lock-in amplifier. In the text, the so-called d^2I/dV^2 curves correspond to the true second derivatives i''. The other ones, which are not corrected, are labeled $V(2\omega)$.

III. ATMOSPHERIC-PRESSURE EXPERIMENTS AND ANALYSIS

A. Barrier Height

The barrier height V_B is determined by measuring the differential capacitance C of the contact at 300 and 77 °K. By plotting $1/C^2$ vs V, a straight line whose intercept with the V axis is V_0 is obtained. V_B is deduced from V_0 by corrections appropriate to degenerate[20] or nondegenerate[21] materials. This procedure implies a knowledge of the Fermi energy μ_F which is easily calculated at 77 °K when only the Γ minimum contains carriers. At 300 °K, both the Γ and L valleys contribute and μ_F is deduced from the calculation of Appendix A. Measurements of 12 vacuum-cleaved n-GaSb–Pb contacts (Table I) provide the values $V_B = 0.55 \pm 0.015$ eV at 300 °K and 0.646 ± 0.009 eV at 77 °K. Only two experimental values of V_B have been reported for n-GaSb–Au contacts[22] ($V_B = 0.61$ eV at 300 °K and 0.75 eV at 77 °K). Our determination is consistent with the fact that on similar III-V compounds, such as GaAs, Au provides larger barrier heights than Pb.[23] The tunnel current must be computed using the value of V_B at 4.2 °K, and we assume that $V_B(T)$ is equal to the variation of the energy gap (~10 meV) between 77 and 4.2 °K.[8] The extrapolated value of V_B is 0.66 eV at 4.2 °K.

B. Differential Resistance

Theoretical and experimental curves of dV/dI, with a zero-bias normalization, are plotted on a linear scale in Figs. 3 and 4. Positive bias corresponds to raising the semiconductor Fermi level with respect to that of the metal.

The differential resistance is calculated in a pure WKBJ approximation[23] using a parabolic barrier and the Franz two-band model.[24] A quadrature over the momentum parallel to the interface is performed and the computation is done using the parameters of Table II. We note that there are some uncertainties concerning the values used in connection with the ⟨111⟩ minima. μ_F is calculated for a parabolic conduction band by the expression given in Appendix A:

$$N=N_0+N_1=\frac{8\pi}{3h^3}(2m_0^*)^{3/2}\left[\mu_F^{3/2}(000)+4\left(\frac{m_d^*}{m_0^*}\left[\mu_F(000)-\Delta E\right]\right)^{3/2}\right]. \qquad (3)$$

For example, μ_F is equal to 84.5 and 93 meV for samples CGSP 5 and 8, respectively. The general features of the curves are similar to the results obtained with GaAs Schottky barriers.[23] The agreement between theory and experiment on the lightly doped sample is remarkable (Fig. 3). On the other hand, experiment and theory (with $\Delta E = 84$ meV) disagree in the over-all shape of dV/dI for sample CGSP 8 (Fig. 4). In the latter sample, the two bands are filled with carriers.

We now anticipate the results of the experiments under pressure (Sec. IV) and assert that we have been able to measure ΔE directly. We estimate $\Delta E = 96 \pm 5$ meV in sample CGSP 8. In principle, this corrected value can be used to recalculate the relation between the Hall coefficient R_H and N (see Appendix A). If this is done, however, the discrepancies between theory and experiment are not reduced and in fact increased somewhat. This probably results from the fact that the Γ band is nonparabolic and that m_0^* at the band edge is quite different from $0.05m$. By carrying out experiments of Hall coefficient and magnetoresistance oscillations, Yep and Becker[15] found a Fermi degeneracy $\mu_F(000) = 104.8$ meV for a sample with

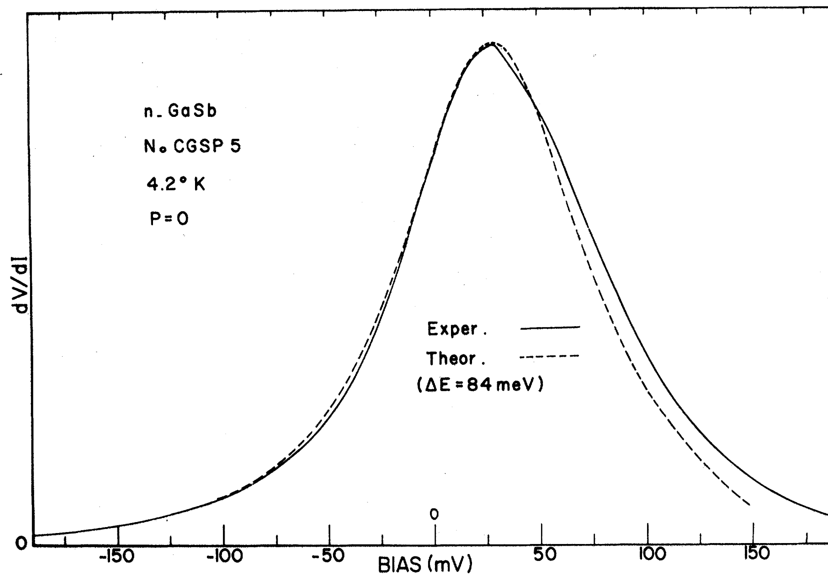

FIG. 3. Normalized incremental resistances dV/dI (arbitrary units) vs bias voltage (lightly doped sample).

the same value of $R_H = -3.35\ \text{cm}^3/\text{C}$ as in sample CGSP 8. Furthermore, they estimated $\Delta E = 95$ meV using the Kane model (nonparabolic band). If we take this result into account, we have

$$\mu_F(000) - \Delta E = \mu_F^0(000) - 84 = \mu_F(111)\ , \qquad (4)$$

where $\mu_F^0(000)$ is the Fermi level in the Γ band. $\mu_F^0(000)$ is calculated by the method of Appendix A (with $\Delta E = 84$ meV). Equation (4) means that the distribution of carriers between the two bands may be deduced with $\Delta E = 84$ meV even if the actual value of ΔE is different. We shall assume that Eq. (4) also holds for other samples.

The theoretical curve for dV/dI with $\Delta E = 96$ meV is shown in Fig. 4. The agreement with experiment is improved but it is not as good as for sample CGSP 5. Uncertainties in the upper-band parameters are not able to explain the disagreement. It seems probable that the tunneling mechanism itself is sensitive to the modifications of the lower band induced by the high doping level.

The experimental and theoretical positions of the resistance maximum V_{max} are, respectively, 28 and 29 mV in Fig. 3 and 47 and 48 mV in Fig.

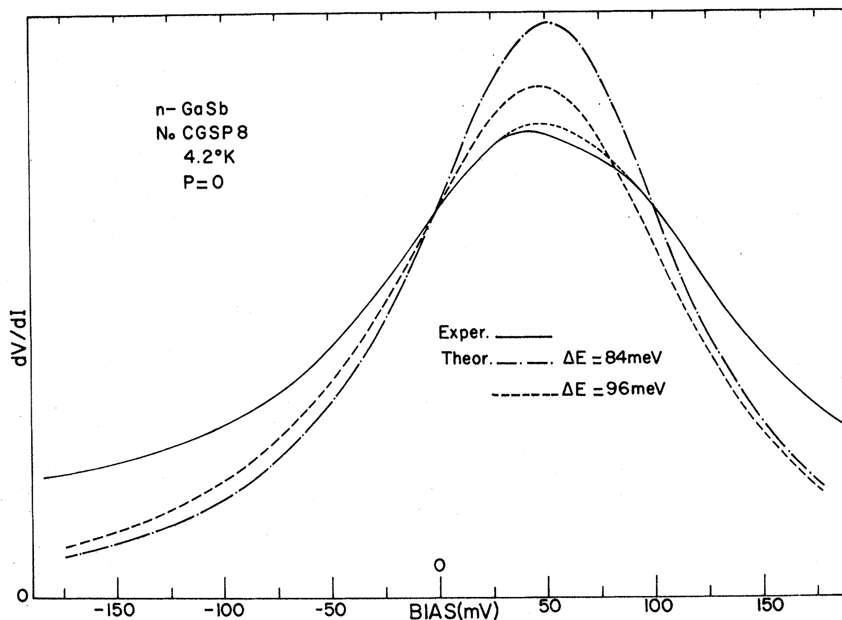

FIG. 4. Normalized incremental resistances dV/dI (arbitrary units) vs bias voltage (heavily doped sample).

TABLE II. Parameters used in the numerical calculation.

Direct-band-gap energy at 4.2 °K[a]	$E_G = 0.813$ eV
Pressure coefficient of the energy gap[b]	$\partial E_G/\partial P = 14.5$ meV/kbar
Energy separation between Γ and L[c]	$\Delta E = E_L - E_\Gamma = (0.084 + 5.9\times10^{-5}T)$ eV
Pressure coefficient of ΔE[d]	$(\partial/\partial P)(E_L - E_\Gamma) = -9.6$ meV/kbar
Effective mass in Γ[c]	$m_0^* = 0.05$ m
Transverse effective mass in L[e]	$m_{1t}^* = 0.1$ m
Anisotropy coefficient in L[e]	$K = m_{1l}^*/m_{1t}^* = 13.5$
Density-of-states effective mass per valley	$m_{1d}^* = 0.238$ m
Conduction-band effective mass in L	$m_{1c}^* = 0.145$ m
Mobility ratio at 300 °K[c]	$\mu_0/\mu_1 = 5.6$
Mobility ratio at 77 °K[c]	$\mu_0/\mu_1 = 9$
Static dielectric constant[f]	$\epsilon_0 = 15.2$
Optical dielectric constant[f]	$\epsilon_\infty = 16.5$
Indirect-gap energy[g]	$L_c - L_v = 2$ eV

[a]S. Zwerdling, B. Lax, K. J. Button, and L. Roth, J. Phys. Chem. Solids 9, 320 (1959).
[b]Reference 35.
[c]C. Y. Liang, J. Appl. Phys. 39, 3866 (1968).
[d]Reference 16.
[e]H. I. Zhang and J. Callaway, Solid State Commun. 6, 515 (1968).
[f]*American Institute of Physics Handbook*, edited by D. E. Gray (McGraw-Hill, New York, 1963).
[g]M. Cardona, Z. Physik 161, 99 (1961).

4. Both theory and experiment in metal-GaAs contacts[23] demonstrated that the influence of N and the related value of μ_F compensate for each other so that V_{max} does not depend appreciably on the doping density. This is not the case in the present experiments and illustrates the fact that the upper valleys limit the increase of $\mu_F(000)$. Another effect, which was also observed in GaAs junctions, is an enhancement of the over-all curvature when N decreases.

The zero-bias resistance R_0 calculated for a metal dot area of 0.33 mm^2 on sample CGSP 5 is equal to 600 Ω, in good agreement with the experimental values (475, 600, and 925 Ω) measured on three diodes. R_0 calculated with $\Delta E = 96$ meV for an area of 0.15 mm^2 on sample CGSP 8 is equal to 0.7 Ω, which is approximately half the experimental value. For the same sample the tunnel current of the carriers in the ⟨111⟩ valleys is about six orders of magnitude lower than the current in the central band.

In conclusion, at zero pressure the main current originates from the specular electron transfer between the metal and the Γ band of GaSb. Theoretical and experimental values of V_{max} and R_0 agree fairly well. The only important discrepancy is observed in the background shape of dV/dI in the most highly doped sample.

C. Plasmon Structure

Structure on the second-derivative curve has been interpreted as an interaction between electrons and plasma oscillations characteristic of the degenerate electron fluid in heavily doped semiconductors. The interpretation of this structure, first observed in GaAs,[25,26] was originally quite controversial.[27–30] The structure is broad and can be considered either as a hump for $V>0$ and a dip for $V<0$, or as an inflexion point for both polarities. GaSb is an interesting material in this respect. The plasmon frequency in bulk n-type GaSb is given by

$$\omega_p^2 = \frac{4\pi e^2}{\epsilon}\left(\frac{N_0}{m_0^*} + \frac{N_1}{m_{1c}^*}\right), \qquad (5)$$

where m_{1c}^* is the conductivity effective mass in the L valleys. Application of pressure leads to a large change in N_0 and N_1, and therefore to a decrease in ω_p. The plasmon structure then appears on different parts of the background resistance curves, which consequently makes it easier to determine its exact line shape. Moreover, the structure can also be readily detected on the first-derivative curves.

The line shape of the dV/dI curves contains a broad dip at forward bias centered at about 37 mV in Fig. 3 and 60 mV in Fig. 4. The over-all agreement between theory and experiment seems sufficiently good in Fig. 3 so that we feel confident in attempting a similar comparison between the second-derivative characteristics of the same sample. The d^2I/dV^2 curves plotted in Fig. 5 help us to extract the exact line shape of the interaction structures. For this study we take advantage of the quasinull zero-bias anomaly which otherwise would severely restrict a clear identification of the structures, especially in junctions prepared by evaporating metal dots on a chemically etched surface.[31] The spectroscopic structures in Fig. 5 can be considered as the superposition of the usual electron-optical phonon interaction in the semiconductor electrode with the plasmon structure.

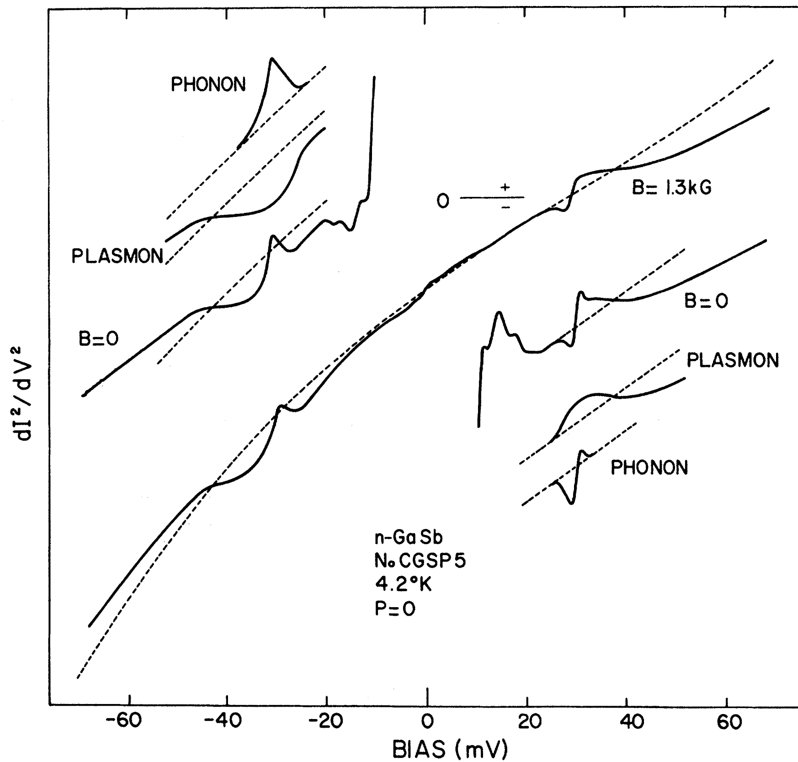

FIG. 5. Experimental (full line) and theoretical (dashed line) curves of d^2I/dV^2 vs bias for $B=0$ and $B=1.3$ kG. The line shape around ± 30 mV appears as the superposition of plasmon and phonon structures.

Figure 5 shows that the plasmon structure is approximately even in conductance. Moreover, for $V>0$ it can be considered as a hump followed by a broad dip (as conjectured from the dV/dI characteristics in Figs. 3 and 4). The simplest way to define the mean energy of this structure is to measure the bias voltage corresponding to the inflection point, i.e., where the theoretical and experimental curves intersect. The corresponding bias changes from ± 40 mV for sample CGSP 5 to ± 59 mV for sample CGSP 8. Using the parameters of Table II and Eqs. (3) and (5), we obtain $\omega_p = 46$ and 60 mV for samples CGSP 5 and 8, respectively. The position of the inflection point is in good agreement with ω_p. We postpone the discussion of these features to Sec. V.

D. Phonon Structure

A characteristic structure in the differential resistance of all metal-semiconductor tunnel junctions has been observed for biases $eV \simeq \pm \hbar\omega_0$, the energy of the approximately zero-k optical phonon in the semiconductor. This structure has been interpreted in terms of self-energy effects in the electrode.

In our data we definitely associate the structure at ± 30 mV with the LO(000) phonon. As for GaAs,[31] the line shape at low temperature, shown in Fig. 6, corresponds to a resistance peak at forward bias and to a double resistance step at reverse bias. The narrow peak is located at 29.4 mV for $V>0$ and 29.6 mV for $V<0$, in good agreement with the phonon energy $\hbar\omega_0 = 29.8$ meV.[32] The affect of thermal broadening is clearly seen in Fig. 5, where the two peaks at reverse bias are not resolved. Care must be taken in interpreting the results since the mixing of the plasmon and phonon structures depends on the doping density. In fact, the line shape and the energy position of the LO structure are quite similar in samples CGSP 5 and 8. The amplitude of the structure, however, increases when the carrier density is lowered (see Table III). Another point (see Table III) is the comparable magnitude of the conductance variation in both voltage directions for a given sample (if we add the contribution of the dip and the peak at forward bias).

In conclusion, the gross features of the tunneling characteristics in GaSb at room pressure are similar to those of GaAs. This is not surprising since both semiconductors are direct-band-gap materials with very similar effective masses ($m_1^*/m \simeq 0.05$ and 0.07 in GaSb and in GaAs, respectively). Moreover, their phonon spectrums are quite comparable. The only difference is that the plasmon structure at $V>0$ can be detected on the first derivative curve in GaSb.

We have reported elsewhere[33] that a low-energy

TABLE III. Relative variation of resistance $\Delta R/R$ owing to the LO(000)-phonon interaction (in %).

Second-derivative structure	Lead state	Sample CGSP 5	Sample CGSP 8
Double peak $V<0$	S^a	2.7	0.65
	N^b	1.3	
Dip, $V>0$	S	1.8	0.32
	N	1.3	
Peak, $V>0$	S	0.4	0.19

[a]Superconducting state. [b]Normal state.

(50-eV) ion bombardment of a chemically etched GaAs surface prior to the metal deposition provides a "cleaning" of the interface. Tunnel characteristics are nearly similar to those of an analogous vacuum-cleaved contact. The same technique applied to GaSb is also characterized by an improvement of the quality of the junctions.[34]

IV. HIGH-PRESSURE EXPERIMENTS AND ANALYSIS

A. Barrier Height

The room-temperature curves of $1/C^2$ vs V remain linear under pressure and their slope changes by only 3–4% between 0 and 15 kbar. This indicates that carrier freeze out is absent under these conditions. The X intercepts V_0 shift towards higher energies. From $V_B = eV_0 + |\mu_F| + kT$,[21] we deduce that $\Delta V_B = e\Delta V_0 + \Delta\mu_F$. The pressure dependence of μ_F is calculated following the method of Appendix A. We again use the parameters of Table II at 300 °K ($\Delta E = 100$ meV, $P_0 = 10.4$ kbar) and the pressure variation of m_0^* is neglected. An important correction is required in order to obtain ΔV_B. For example, at $P=0$, $\mu_F(000) = -6$ meV and above P_0, $\mu_F(111) = -87$ meV. A satisfying feature of the results shown in Fig. 7 is the linearity of $\Delta V_B(P)$ obtained in this way. For $P<P_0$, $\partial V_B/\partial P = 15.7 \pm 0.4$ meV/kbar, which com-

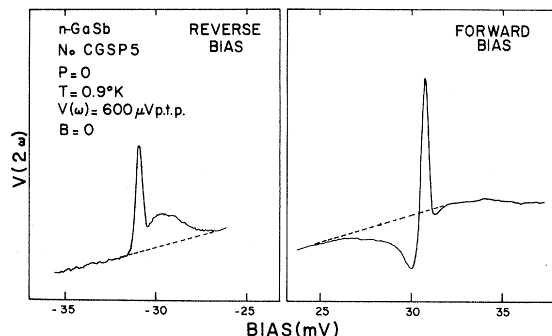

FIG. 6. Enlarged view of the optical phonon structure at 0.9 °K in a cleaved sample (p.t.p. stands for peak to peak).

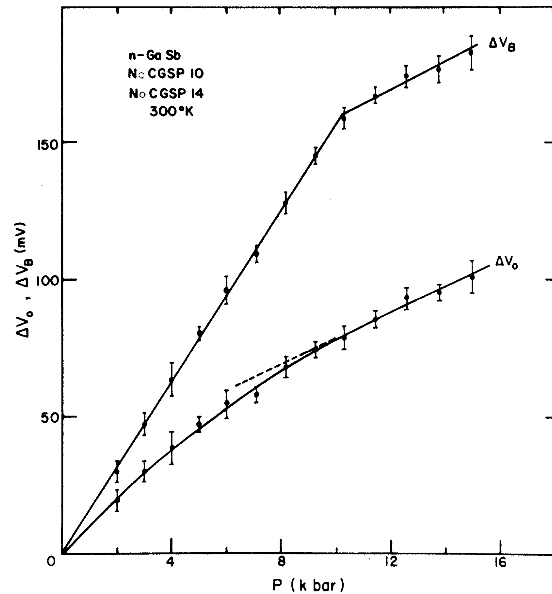

FIG. 7. Pressure dependence of V_0: the intercept of the $1/C^2$-vs-V curve with the V axis, and of V_B: the barrier height.

pares fairly well with the direct-gap coefficient $\partial E_G/\partial P = 14.5$ meV/kbar.[35] For $P>P_0$, $\partial V_B/\partial P = 5.2 \pm 1$ meV/kbar, which corresponds closely to the expected shift of the $\langle 111\rangle$ minimum. Once again we may conclude that, as for GaAs,[17] the Fermi level at the interface remains pinned with respect to the valence band when the pressure increases. Thus, our measurements constitute the most direct determination of the pressure coefficient of the L valleys in GaSb.

B. Background Resistance

The computation of the differential resistance is carried out in the same way as in Sec. III B except that we now introduce the pressure dependence of E_G, ΔE, V_B, and μ_F. $\partial V_B/\partial P$ is taken to be independent of T and we make use of our prior experimental values. A typical plot of $\mu_F(000)$ and $\mu_F(111)$ vs P is shown in Fig. 8. The plot illustrates the decrease of $\mu_F(000)$ which results from the progressive depletion of the $\langle 000\rangle$ valley and the corresponding accumulation in the $\langle 111\rangle$ valleys. Depending on the actual value of the intervalley gap ΔE, to be determined by experiment, the Fermi level $\mu_F(000)$ is deduced using Eq. (4). At $P=P_1$, the $\langle 000\rangle$ band becomes totally free from carriers so that $\mu_F(111)$ remains practically constant and is solely determined by the parameters of the $\langle 111\rangle$ valleys. The energy gap is taken to be 2 eV at the Brillouin-zone boundary in the L direction. The current is calculated for the two ellipsoids, the $\langle 111\rangle$ axes of which are in the plane of

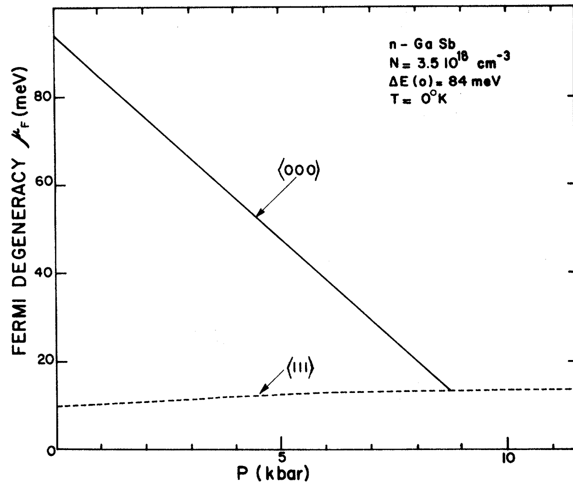

FIG. 8. Typical variations of $\mu_F(000)$ and $\mu_F(111)$ with the applied pressure at 0 °K.

the junction. The tunneling mass is then equal to $m_{1t}^* = 0.1m$, where m is the mass of the free electron. The orientation of the two other L valleys is less favorable and their higher tunneling mass leads to a negligible contribution to the total current. Typical dV/dI data under pressure are shown in Figs. 9 and 10. The vertical logarithmic scale gives the absolute value of the experimental resistance. The theoretical curves have been normalized at zero bias. Using experimental results to be described, we performed the calculation with room-pressure values of ΔE equal, respectively, to 100 and 110 meV for samples CGSP 7 and 1. The most striking features of the plots are (a) the huge increase of resistance and (b) the strong variation of the shape of dV/dI. Both are the consequences of the progressive depletion of the central band. The agreement between theory and experiment can be considered as satisfactory except at the highest pressures where other effects occur. We discuss them in what follows.

We now consider the variation of V_{max} and the evolution of R_0. The pressure dependence of V_{max}, shown in Fig. 11, is analyzed as follows. At low pressure, when $\mu_F(000)$ is larger than the "characteristic energy"[24] $E_0(000)$ and $V_B/E_G > 0.5$, the incremental resistance does not peak at a bias equal to μ_F. For example, in sample CGSP 7, $\mu_F(000) = 110$ meV, $E_0 = 39$ meV, and $V_B/E_G = 0.81$. The shift of V_{max} towards higher voltages is the result of the combined variation of V_B, E_G, and μ_F. This effect is qualitatively similar to what was obtained in n-GaAs tunnel contacts.[17] Nevertheless, as soon as μ_F becomes comparable with E_0, V_{max} decreases and moves towards μ_F. This is clear at 10 kbar when $\mu_F(000)$ is reduced to 20 meV. Above P_0, the central band becomes almost completely depleted. The resistance increases sharply around P_1, and beyond P_1 the current is due to carriers in the ⟨111⟩ valleys. Appropriate parame-

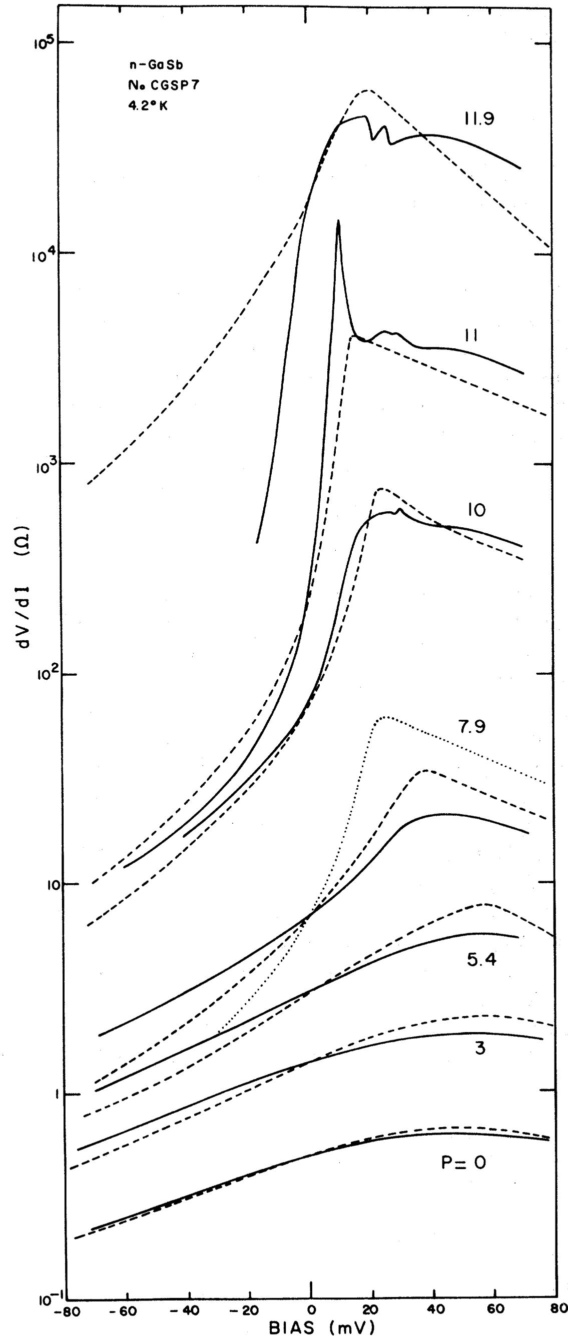

FIG. 9. dV/dI on a logarithmic scale vs bias voltage at different pressures (in kbar). Full lines, experimental curves; dashed lines, theoretical curves normalized at zero bias to the experimental ones and calculated with $\Delta E(0) = 100$ meV; dotted line, theoretical curve calculated with $\Delta E(0) = 84$ meV. The computation has been performed with the ⟨000⟩ band parameters up to 11 kbar and with the ⟨111⟩ valley parameters at 11.9 kbar.

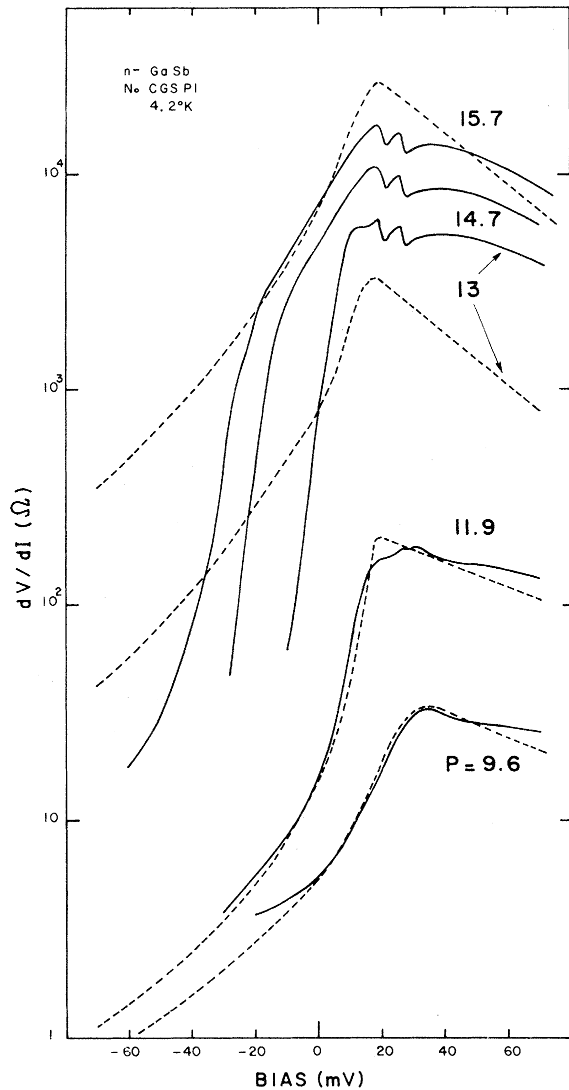

FIG. 10. dV/dI on a logarithmic scale vs bias voltage at different pressures (in kbar) for the most heavily doped sample. Full lines, experimental curves; dashed lines, theoretical curves normalized at zero bias to the experimental ones and calculated with $\Delta E(0) = 110$ meV. The computation has been performed with the ⟨000⟩ band parameters up to 11.9 kbar and with the ⟨111⟩ valley parameters at higher pressures.

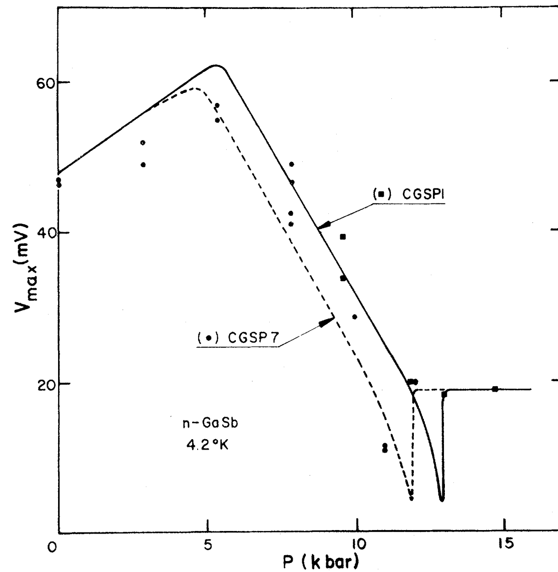

FIG. 11. Theoretical pressure dependence of V_{max} (pure specular tunneling) and experimental data.

ters are then $\mu_F(111) = 15$ meV, $E_0(111) = 27$ meV, and $V_B/E_G(111) = 0.41$. We then have $eV_{max} = 19$ meV at all pressures $P > P_1$.

The theoretical and experimental variations of $R_0(P)$ are shown in Fig. 12. The theory predicts, and the experiment confirms, a strong increase of R_0 around $P = P_1$ resulting from a sudden change in the tunneling mass. This provides a first estimate of P_1 equal, respectively, to 12 and 13 kbar for samples CGSP 7 and 1. For $P < P_1$, the quantitative agreement is excellent for sample CGSP 7 and

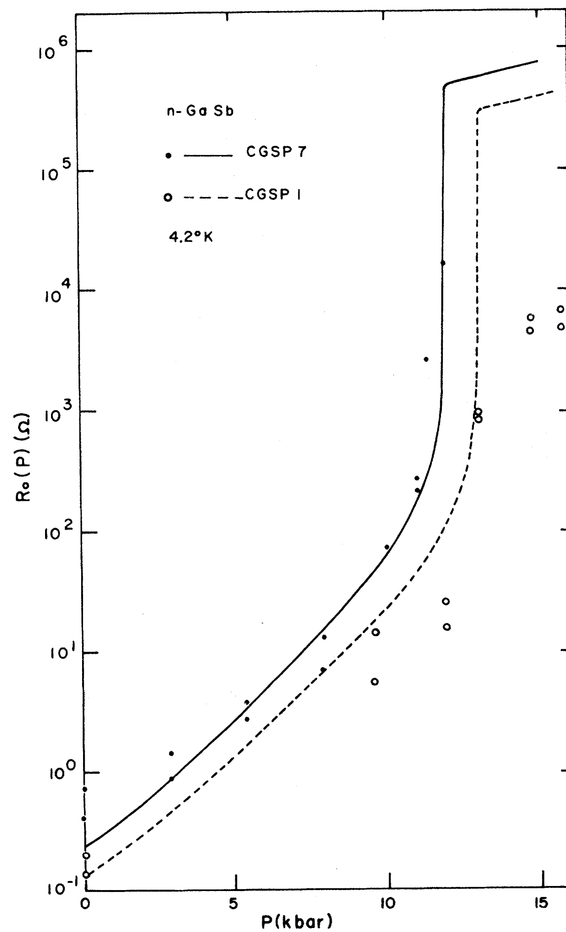

FIG. 12. Theoretical pressure dependence of the zero-bias resistance and experimental data.

satisfactory for sample CGSP 1. Above P_1 there is a marked discrepancy which suggests the onset of an additional current mechanism in parallel with the specular channel.

C. Plasmon Structure

The logarithmic plot in Fig. 9 is not convenient for observing the pressure dependence of the plasmon structure. The shift of this structure is more clearly depicted on the linear plot of dV/dI versus forward bias in Fig. 13. Above 8 kbar the broad resistance dip is buried into the superconducting density-of-states structure at low bias voltages. The pressure dependence of the experimental position of the inflexion point of d^2I/dV^2 for $V>0$ is plotted in Fig. 14 together with the theoretical variation of ω_p calculated by Eq. (5). At low pressure, the agreement between these two quantities is very good. We discuss in Sec. V the possible origin of the discrepancies which are observed above 5 kbar.

D. Band-Crossing Anomaly

An unexpected feature in Fig. 9 consists in the appearance of a sharp resistance peak superimposed on the background curve at 11 kbar. This

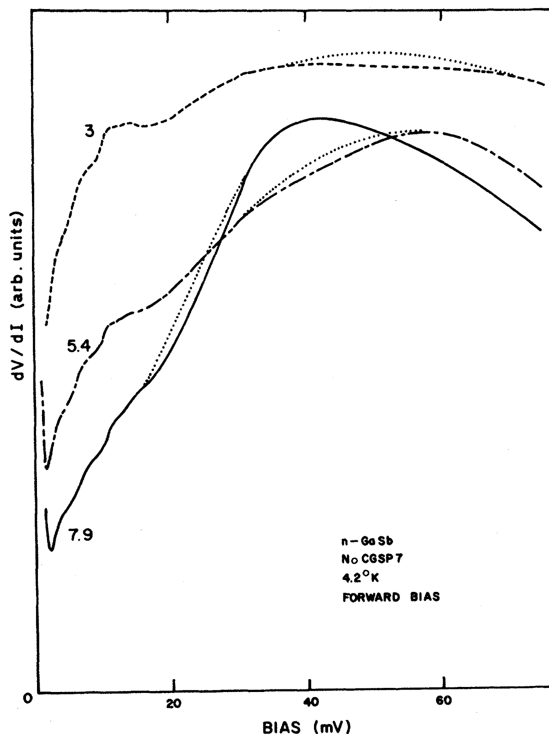

FIG. 13. dV/dI (different arbitrary units for each curve) vs bias voltage at 3, 5.4, and 7.9 kbar showing the broad resistance dip attributed to the electron-plasmon interaction in the semiconductor electrode. Dotted lines represent interpolated backgrounds.

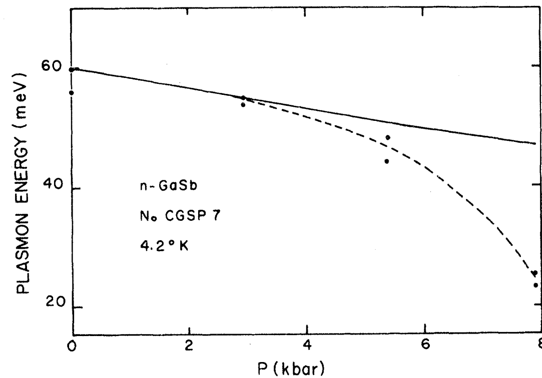

FIG. 14. Theoretical pressure dependence of ω_p (full line) and experimental points. The dashed line represents the estimated experimental variation.

anomaly, shown on a magnified plot (Fig. 15), can be described as follows: (i) It occurs only at forward bias around 10–15 mV, (ii) its position in energy decreases when P increases, (iii) the width of the peak can be as narrow as 2 mV at half-height, and (iv) the pressure must verify $P_0 \leq P < P_1$. In other words, this structure appears beyond the band crossing but below the pressure at which the central band is completely depleted of electrons. Moreover, the peak is centered at $eV_{max} \simeq \mu_F(000)$. We show in Appendix B that this behavior can be attributed to the reflection of the superconducting Pb gap at the sharp resistance increase which occurs between $V=0$ and $eV=\mu_F(000)$. This is somewhat analogous to the behavior of the electron–LO-phonon structure when the metal is in the superconducting state: the LO structure is modulated by the superconducting density of states. In the present case the anomalous strength of the effect is due to the huge resistance change between $V=0$ and $eV=\mu_F(000)$. When P increases, $\mu_F(000)$ and the position of the resistance peak (Fig. 15) decrease. Moreover, the larger the resistance step is, the larger the amplitude of the anomaly (11 kbar). The calculation predicts the magnitude of this effect rather well. Since no magnetic field was applied during these experiments, we cannot ascertain whether or not superconductivity is the reason for this anomaly. Nevertheless, during the cooling of the pressure bomb we observed that the resistance peak was noticeable only for $T<T_c$, where T_c is the superconducting transition temperature.

E. Resistance Kink

We have already reported[6] that one of the most interesting features of the curves at high pressure consists in a sharp resistance kink occurring at reverse bias. Consider now the differential resistance at 15.7 kbar computed with the $\langle 111 \rangle$ band parameters (Fig. 10). We observe that the agree-

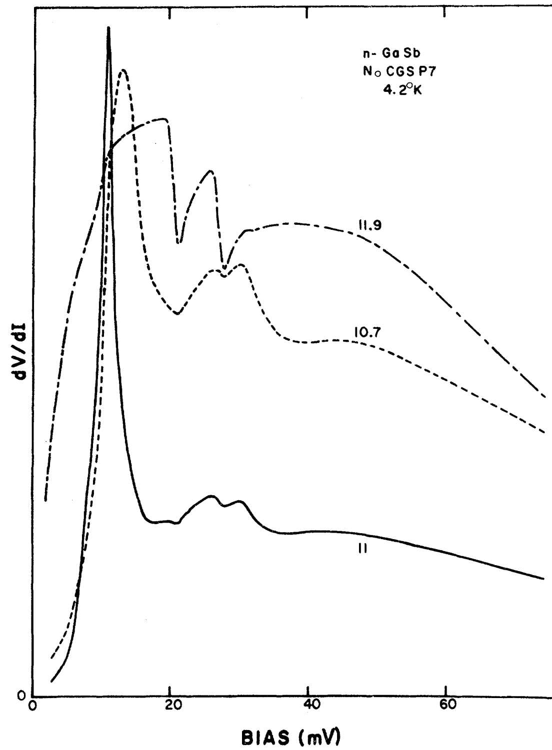

FIG. 15. dV/dI (different arbitrary units for each curve) vs bias voltage at 10.7, 11, and 11.9 kbar showing the band-crossing anomaly around 10–15 mV at forward bias.

ment between theory and experiment is fairly good at reverse bias up to a threshold voltage where tunneling into the central band begins. Figure 16

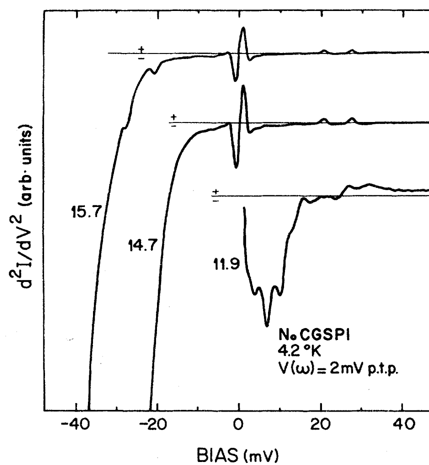

FIG. 16. d^2I/dV^2 vs bias voltage for 11.9, 14.7, and 15.7 kbar showing the onset of tunneling in the ⟨000⟩ valley. The superconducting zero-bias structure is smoothed by the relatively large voltage modulation (p.t.p. stands for peak to peak).

shows that the resistance kink manifests itself as a nearly vertical drop of d^2I/dV^2; the higher the pressure, the more negative the corresponding threshold. This voltage is a direct measure of $E_L - E_\Gamma + \mu_F(111)$. The kink occurs at $V = 0$ when $P = P_1$. This provides us with another estimate of this critical pressure. Again we find $P_1 = 12$ and 13 kbar for samples CGSP 7 and 1, respectively. Below P_1, however, a similar rapid variation of d^2I/dV^2 still occurs at $V > 0$. The main current comes from the ⟨000⟩ valley for which $E_0 \gg \mu_F(000)$. A sharp resistance increase occurs approximately at $V \simeq \mu_F(000)$. At $P \leqslant P_1$ we therefore measure $\mu_F(000)$ and calculate ΔE. The plot of the threshold voltage shown in Fig. 17 leads to an interband coefficient $\partial\Delta E/\partial P = -9.6 \pm 1$ meV/kbar in close agreement with a previous experimental determination.[16]

The onset of tunneling into the central band has a sensitive effect on the I-V characteristics shown in Fig. 18. Let us compare the forward bias curves at 0 and 13 kbar. In sample CGSP 1, we observe that the influence of the high doping level is compensated by the low tunneling probability resulting from the dispersion law of the ⟨111⟩ valleys. The net result is that the current in both samples is of the same order of magnitude. Conversely, at reverse bias the onset of tunneling in the central band leads to a strong asymmetry of the high-pressure curve. This effect is quite similar to the "Kane kink" in germanium p-n tunnel diodes.[36]

F. Zone-Boundary Phonons

We now consider the phonon structure. The description can be divided in two parts. First,

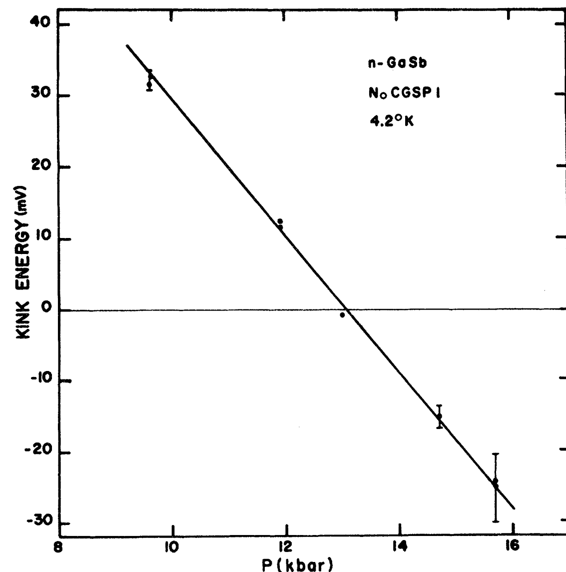

FIG. 17. Pressure dependence of the "kink" energy. The slope of the curve, equal to -9.6 ± 1 meV/kbar, provides a direct experimental measurement of $\partial(\Delta E)/\partial P$.

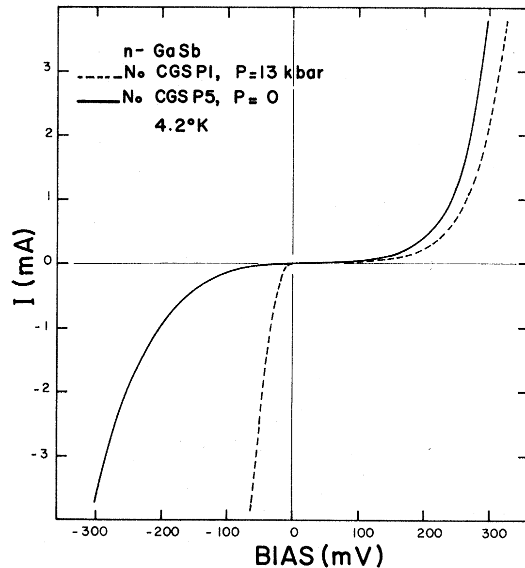

FIG. 18. Current-vs-voltage characteristics showing the strong asymmetry resulting from the onset of tunneling into the central band at high pressure.

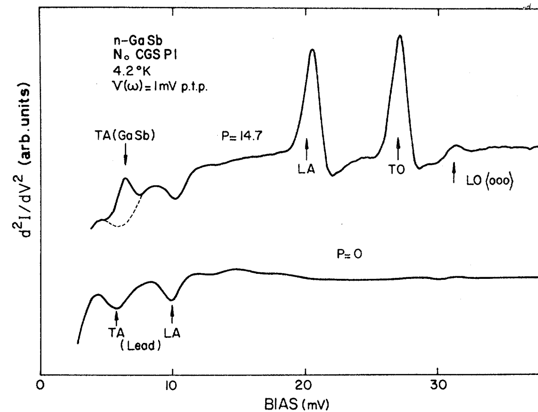

FIG. 20. d^2I/dV^2 vs forward voltage for $P=0$ and $P=14.7$ kbar showing the inelastic structures and the tentative phonon indexation (p.t.p. stands for peak to peak).

zone-edge phonon-assisted processes appear around $P=P_0$ and above. Second, we observe a modification of the line shape and magnitude of the electron–LO-phonon interaction when the pressure increases.

It is known that at low temperature, sharp thresholds appear in the experimental I-V characteristics of p-n tunnel diodes in indirect semiconductors. These thresholds were initially identified[37,38] as owing to the emission of a phonon by the tunneling electron in order for the tunneling process to satisfy conservation of momentum. As the electron loses energy to the emitted phonon, the bias voltage must equal or exceed the phonon energy.

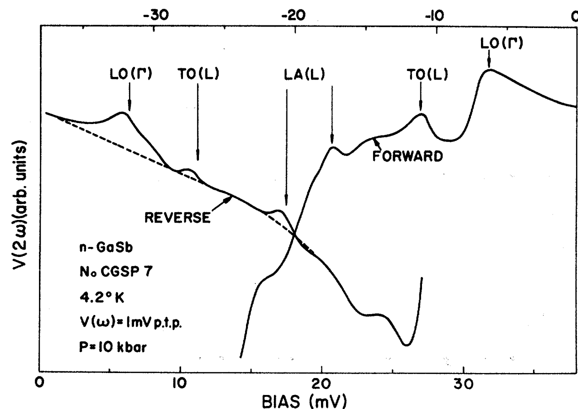

FIG. 19. Magnified plot of $V(2\omega)$ vs bias voltage showing the parity of the phonon structures at 10 kbar.

In n-Ge Schottky barriers, the metal Fermi surface is large enough to allow direct (specular) tunneling without violation of the parallel momentum conservation rule. Then, most of the current flows by the direct channel in which no phonon emission occurs. Nevertheless, another channel for the current is the phonon-assisted tunneling[4,5] which is quite similar to what occurs in p-n junctions. The first step is the injection of electrons from near the forward direction ($k_{\parallel}\approx 0$) of the metal Fermi surface into states associated with the Γ conduction band. For the bias voltages of interest these states are at an energy below the Γ conduction band edge and are thus evanescent in the semiconductor (Fig. 1). During the second step, the tunneling channel for the electron is completed by the emission of a phonon of wave vector $q\simeq(-\pi/a)(1,1,1)$, allowing the electron to make a transition from the state of Γ symmetry to a current-carrying state of symmetry L at $k=(\pi/a)(1,1,1)$. A similar two-step process occurs when the Ge electrode is biased negative relative to the metal.

In GaSb, above $P\simeq P_0$, we detect the appearance of zone-boundary phonon-assisted tunneling. The corresponding structures[6] are well resolved on the curves at the highest pressures, even on the first-derivative plots (Figs. 9 and 10) where they appear as resistance "down" steps. One of the most remarkable features of the present results concerns the line shape of the structures at $V<0$. Figure 19 shows a magnified plot of $V(2\omega)$ at 10 kbar. Whatever the actual background at $V<0$, the main structure of the zone-edge process is essentially a *peak*. Nevertheless, if we consider the results of Fig. 16, we observe that for $V<0$ the two main structures at the highest pressure appear as *dips* on the background curve. A careful analysis of our data leads to the conclusion that the line

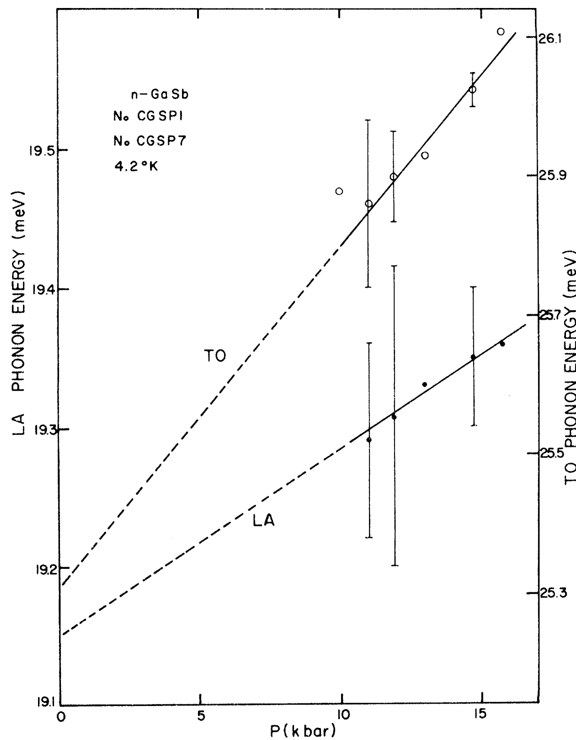

FIG. 21. Pressure dependence of the LA(111)- and TO(111)- phonon energies.

shape depends on the value of ΔE with regard to the energy of a given phonon $\hbar\omega_L$. Beyond the band crossing, the transition from a peak to a dip, at reverse bias, occurs at the pressure for which the resistance kink energy $|E_\Gamma + \mu_F(111) - E_\Gamma|$ is equal to $\hbar\omega_L$.

The zone-boundary phonon structures are clearly displayed in Fig. 20. Starting from $V=0$, the first is found at 5.3 mV ($\Delta R/R = 7\%$) and mixes with the lead TA-phonon structure. The positions of the next two peaks have been studied under pressure (Fig. 21). An extrapolation to $P=0$ leads to the values of Table IV which contains the main phonon data obtained from our experiments. The major uncertainty concerns the TA(111)-phonon energy.

The pressure dependence of the magnitude of the LA and TO inelastic structures (Fig. 22) reveals a strong increase of $\Delta R/R$ between 12 and 13 kbar for sample CGSP 1 and between 11 and 12 kbar for sample CGSP 7. This is another indication of the value of P_1 since we expect $\Delta R/R$ to be large as soon as the contribution of the central band to the tunnel current vanishes. Owing to the contribution of direct tunneling into the central band for $V<0$, $\Delta R/R$ is generally weaker than for $V>0$.

G. LO(000)-Phonon Structure

The characteristic tunnel structure related to the electron-LO(000)-phonon interaction contains certain features which are not clear at the present time. Cullen *et al.*[39] have carried out experiments on *p*-type Si. In particular, they investigated the systematic modification of the tunneling curves with changes in the doping density N. They concluded that the origin of various aspects of the curves are not completely understood for all N values. The application of pressure constitutes a convenient way of continuously varying $\mu_F(000)$ and N_0 in the Γ band. This in turn has a drastic influence on the line shape, parity, and magnitude of the phonon structure.

Figure 23 presents a general survey of the second-derivative characteristics for a large range of pressures. At a forward bias of ~ 30 mV at low pressure we recognize the LO(000)-phonon structure, which is composed of a dip and a peak. Above 5.4 kbar *the peak disappears*. At $P>10$ kbar this structure exhibits a strong modification in the sense that the *dip* becomes a single *peak* which looks like a usual inelastic process. Under reverse bias the LO-phonon-structure line shape is relatively insensitive to changes in μ_F.

The pressure-dependent position of the LO-phonon structure at $V>0$ is estimated to $\partial\hbar\omega_0/\partial P = 12 \pm 2.10^{-5}$ meV/kbar. At 11 kbar the peak occurs at $+30.4 \pm 0.3$ mV. It can be considered as the corresponding of the peak in the $P=0$ line shape.

The magnitude of the structure at $V>0$ was only studied at high pressure, i.e., when it appeared as a single peak. Figure 24 shows that $\Delta R/R$ increases sharply (up to 25%) around $P=P_0$. At reverse bias (Fig. 25) the magnitude is different and does not peak at the same pressure.

H. Multiphonon Structures

During the course of these experiments a search in a bias region ±100 mV was also made for peaks in the d^2I/dV^2-vs-V curve other than those treated in detail. At high pressure two additional structures appear at biases which correspond to a double-phonon emission LA(111) + LO(000) and

TABLE IV. Phonon-structure energies at room pressure in GaSb from tunneling spectroscopy.

Phonon indexation	Bias	Temperature (°K)	Shape	Energy (meV)
LO(000)	Direct	4.2	Dip	28.3 ± 0.4
			Peak	29.8 ± 0.3
	Reverse			29.4 ± 0.2
	Direct	0.9	Dip	28.8 ± 0.2
			Peak	29.5 ± 0.2
	Reverse			28.3 ± 0.2
				29.6 ± 0.2
TA(111)	Direct	4.2		5.3 ± 0.5
LA(111)				19.15 ± 0.2
TO(111)				25.3 ± 0.2

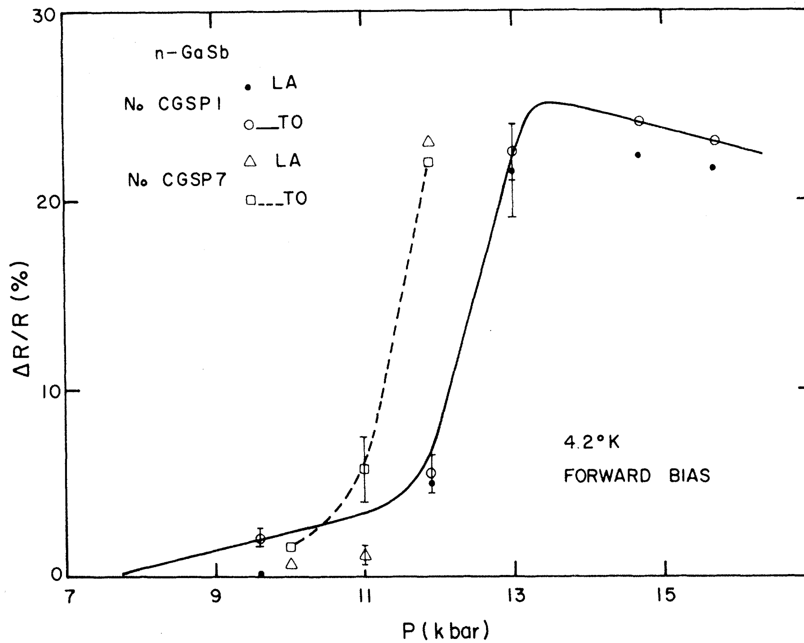

FIG. 22. Variation of the magnitudes of the LA(111)- and TO(111)-phonon structures with the applied pressure at forward bias.

TO(111) + LO(000). Such a process has been already reported in the case of p-n tunnel junctions.[40] The magnitude of the structures (~0.7% at 14.7 kbar) corresponds fairly well to the product of the values of $\Delta R/R$ relative to the phonons involved in the double-emission mechanism.

V. DISCUSSION

A. Band Structure of GaSb

All preceding results converge P_1 values equal to 12 and 13 kbar in samples CGSP 7 and 1, respectively. From the calculated value of $\mu_F(111)$, we deduce that $P_0 = 10.5$ and 11.5 kbar, and $\Delta E(0) = 100$ and 110 meV, respectively. When introduced into the computation of the tunnel current, these parameters provide fairly good agreement between theory and experiment. Although the doping level might be slightly inaccurate, it appears that ΔE increases with the carrier density. The same conclusion was inferred by Fritzche and Tiemann[41] from their experiments in p-n Ge junctions. ΔE was measured 15 meV larger than the value for pure material. On the other hand, our results are in contradiction with those of Tongerloo and Woolley,[12] who found $\Delta E(0) = 75$ meV for $N = 2\times 10^{18}$ cm^{-3}. The computation of the tunnel current demonstrates that the excellent agreement between theory and experiment in sample CGSP 5 is proof that $\Delta E(0) \geq 85$ meV for this N value. Moreover, the same authors found a decrease of $\Delta E(0)$ with N which is opposite to our conclusions. It is worth pointing out that ΔE is measured *directly* in our experiments and not deduced from several indirect methods. We have no clear idea of the exact mechanism which leads to this rather strong dependence on N.

B. Background Resistance

The general agreement between theory and experiment for both the shape and magnitude of the tunneling curves is excellent (Figs. 9–12). The main discrepancies between the theoretical and experimental resistances occur at high pressure (Fig. 12). The observed resistance is roughly 75 times smaller than the computed one. It is clear that a new tunnel mechanism is responsible for this large disagreement. We suggest that the main current is assisted by the ionized impurities in much the same way as it is assisted by the zone-edge phonons when the bias is sufficiently large. In fact, this kind of impurity-assisted tunneling provides the quantitative interpretation of the finite zero-bias conductance of Ge Esaki diodes.[42] Diffusion by the charged impurities may induce intervalley transitions which correspond to new (two-step) tunneling channels where the electrons are transmitted through the barrier with the characteristics of the Γ valley.

C. Plasmon Structure

Our experiments tend to confirm that the plasmon structure on the second-derivative curves cannot be simply treated as a hump at $V > 0$ and a dip at $V < 0$. Therefore, the interaction cannot be interpreted as a pure inelastic process. At low pressures, the bulk value of ω_p agrees fairly well with the energy of the inflexion point taken as the

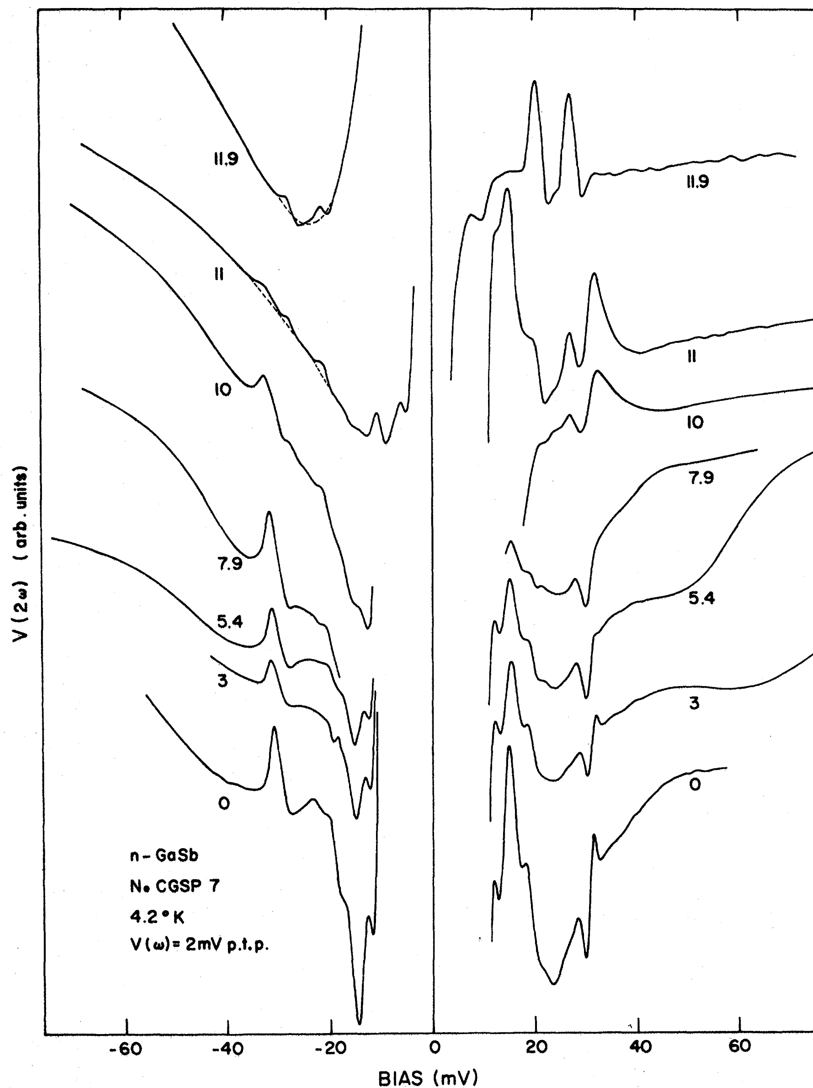

FIG. 23. Evolution of the second-derivative characteristics when pressure increases from 0 to 11.9 kbar. The superconducting structures near the zero bias have been omitted for clarity. All structures below $|V| \simeq 20$ mV are due to the harmonics of the lead phonons. The LO(000)-phonon structure is situated at ± 30 mV. At high pressure (11 and 11.9 kbar) the zone-boundary phonon structures show up.

center of the line. At high pressures, the disagreement between theory and experiment seems too large to be due solely to the inaccuracy of parameters of the upper valley. Furthermore, a LO-phonon–plasmon coupling cannot be invoked to explain a shift of the plasmon energy. Indeed, we observe that ω_p has the same value for sample CGSP 7 at 7.9 kbar and for sample CGSP 5 at $P=0$; in the latest case, the LO phonon is at the correct bias compared to the pure bulk phonon energy. An additional experimental detail may help us in finding reasonable interpretation. In Fig. 23 the curve at 7.9 kbar has an inflexion point at -44 mV (not far from the theoretical value of ω_p) instead of at $+23$ mV. We thus believe that the observed disagreement at forward bias comes from the decrease of μ_F. For $\mu_F < \hbar\omega_p$ we expect a disappearance of the dispersive part of the electron-plasmon interaction at *forward bias*. Our experi-

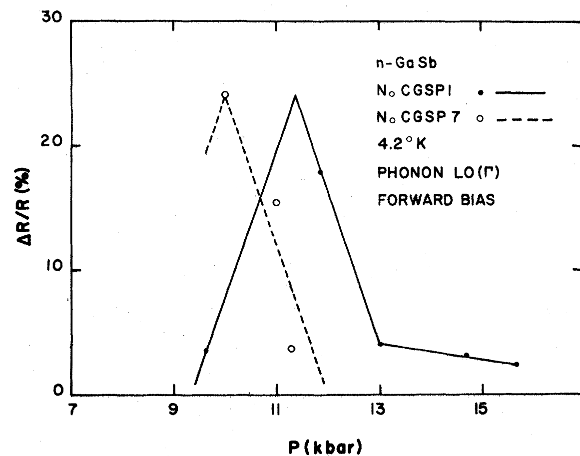

FIG. 24. Variation of the magnitude of the LO(Γ)-phonon structure with pressure at forward bias.

ments agree with this expectation ($\mu_F = 35$ meV at 7.9 kbar) and reinforce the idea that the actual mechanism may be essentially an electrode self-energy effect instead of a surface-plasmon emission by the electrons when they are tunneling through the barrier. However, we do not understand why a large resistance dip still remains around 23 mV at 7.9 kbar. It is a difficult task to depict the plasmon structure at higher pressure.

D. $k \sim 0$ Phonon

We have already mentioned that the line shape of the structure attributed to the $k \sim 0$ phonon-electron interaction is similar in GaAs and GaSb. At $V > 0$ the peak corresponds fairly well to the LO(000)-phonon energy. The question arises as to whether the TO phonon could also play a role and contribute to the line shape. If so, the magnitude of $\delta E = \hbar\omega_{\rm LO} - \hbar\omega_{\rm TO}$ should be of some importance: $\delta E = 3$ and 1.2 meV for GaAs and GaSb, respectively. Since our experiments have shown that the energy difference between the dip and the peak is approximately the same in both materials (1.5 – 1.8 meV), we believe that the TO(000) phonon is not detected in GaAs and GaSb n-type compounds. The present experiments allow for other important conclusions about the influence of some parameters on the LO structure. We have already reported[17] that a modification of the barrier shape following the application of hydrostatic pressure in metal-GaAs tunnel junctions yielded a change of the magnitude but *not* of the line shape of the structure. Among those semiconductors which have been used in Schottky-barrier tunneling, GaSb is unique in the sense that in it N can be varied while μ_F is kept approximately constant. Conversely, we can vary μ_F and keep N constant. The first case is illustrated by a comparison between samples CGSP 5 and 7 at $P = 0$, in which μ_F is, respectively, 84 and 94 meV and the N values (Table I) are quite different. We mentioned that the magnitude but *not* the line shape of the structure was influenced by N. This is probably due to the screening of the electron-phonon interaction by the carriers. The second possibility is illustrated by sample CGSP 7 under pressure when μ_F progressively decreases. We have shown that at *forward bias* the line shape is strongly modified by the decrease of $\mu_F(000)$. At $P = 0$, the line shape corresponds essentially to the dispersive part of the self-energy. Indeed, it has been calculated[42] that the main feature of this component is the same both in the barrier and in the electrode and that it always appears as a conductance dip at $V > 0$. This leads to the characteristic dip and peak structure shown in Fig. 6. At 10 kbar $\mu_F(000) = 20$ meV $< \hbar\omega_0$ and the dispersive terms vanish (forward bias). However, a dissipative phonon emission in or near the barrier can still occur and the structure appears as an inelastic process, i.e., a peak at forward bias (Fig. 23). Between $P = 0$ and $P = 10$ kbar ($\mu_F > \hbar\omega_0$), the phonon structure exhibits a strong modification. For example, at 5.4 and 7.9 kbar, the line shape is reduced to a single dip, i.e., a conductance down step. This particular feature necessarily involves the existence of a *negative* dissipative contribution. To our knowledge, this is the first experimental evidence for a step decrease of the conductance related to an electron-phonon interaction. The theoretical interpretation of this effect is presently under study.

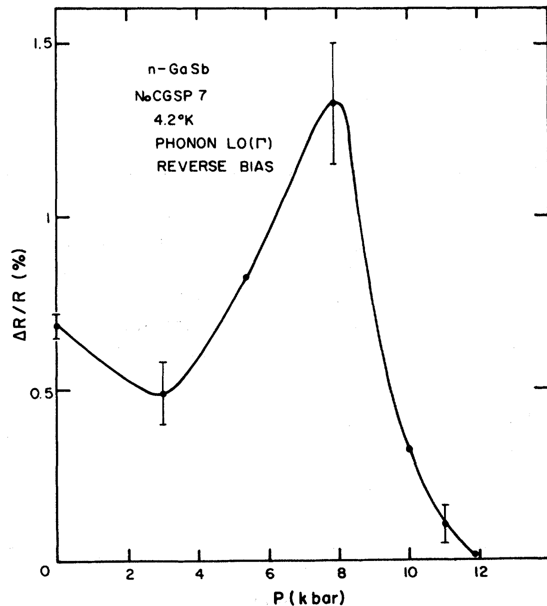

FIG. 25. Variation of the magnitude of the LO(Γ)- phonon structure with pressure at reverse bias.

We now turn to a discussion of the magnitude of the phonon structure. One of the striking features in Fig. 24 is the large value of $\Delta R/R$ around 10 kbar in sample CGSP 7 and 11 kbar in sample CGSP 1. Since the electron-phonon interaction is independent of m^* and since the screening does not vary much when the carriers are transferred into the $\langle 111 \rangle$ valleys, we believe that this phenomenon is related to the particular shape of dV/dI around 10 kbar (Fig. 9). $\Delta R/R$ is given by

$$-\frac{\Delta R}{R} = \frac{\Delta G_p}{G(\hbar\omega_0)} \equiv \frac{\Delta G_p}{G(0)} \; \frac{G(0)}{G(\hbar\omega_0)} \;, \qquad (6)$$

where ΔG_p is the additional conductance owing to the electron-phonon interaction. $G(0)$ and $G(\hbar\omega_0)$ are the background conductances at $V = 0$ and $eV = \hbar\omega_0$, respectively. It can be qualitatively shown[42] that $\Delta G_p / G(0)$ is rather independent of the

pressure around $P=P_0$. At the highest pressures, $G(0)/G(\hbar\omega_0)\simeq 1$ and one measures $\Delta G_p/G(0)$. When the pressure is decreased towards P_0, the conductance varies strongly between $V=0$ and $eV=\hbar\omega_0$ (Fig. 9). In this situation, the magnitude of $\Delta G_p/G(0)$ is amplified by the factor $G(0)/G(\hbar\omega_0)$, which can reach 20.

The line shape at $V<0$ is unchanged by the pressure increase and the magnitude of $\Delta R/R$ is lower than at $V>0$. The variation of $\Delta R/R$ is more difficult to interpret and seems related to the value of $\mu_F(000)$.

E. Zone-Boundary Phonons

Tunneling under pressure in GaSb provides the first experimental determination of the zone-edge phonon energies in the $\langle 111\rangle$ direction. The first two structures in Fig. 20 unambiguously correspond to the TA(111) and LA(111) modes, in good agreement with their predicted energies.[43] By comparison with GaAs, the third structure is most likely due to the TO(111) phonon. Therefore, either no LO(111) structure appears or it is obscured by the other peaks.

The particular features of the line shape at $V<0$ can be roughly interpreted as follows. In case (a), we have

$$|E_\Gamma+\mu_F(111)-E_L|<\hbar\omega_L \qquad (7)$$

for a given phonon; conversely in case (b). *At forward bias*, electrons originating from the L minimum can emit a zone-boundary phonon and transfer to an intermediate state of the Γ valley. This mechanism probably occurs in the immediate vicinity of the boundary between the barrier and the semiconductor electrode. It is a purely dissipative effect which enhances the tunneling current and is present in case (a) and case (b) as well. *At reverse bias*, electrons originating from the metal along the Γ dispersion curve are transferred into the L valley in a similar way. The difference between both cases is the following: In case (a) the Γ valley has a definite density of states at the relevant energy so that the dispersive and dissipative effects occur simultaneously, while in case (b) the density of states is zero and the effect is purely dissipative.

Finally, let us compare our results to those obtained in Ge Schottky barriers[5] where four phonon structures were resolved. A temperature effect may be invoked to explain this result. If so, in p-n junctions[40] at 4.2 °K the LO(111)-phonon structure (of medium amplitude) is buried in the LA(111)-phonon line shape. Another possibility is a degeneracy of the LO and TO branches at the zone-boundary along the $\langle 111\rangle$ direction.

In both Ge and GaSb the LA(111)-phonon structure is strong ($\Delta R/R=10\%$ in Ge[5] and 25% in GaSb at 13.5 kbar). Nevertheless, Ge and GaSb cannot be compared in a straightforward manner. Indeed, $\Delta R/R$ depends on m_0^*, m_{1c}^*, N, and V_B. On the other hand, it is easy to understand the influence of ΔE. Beyond P_1 at very high pressures the barrier height corresponding to the Γ valley increases faster than that of the L valleys. Therefore, the Γ tunneling path becomes progressively less favorable for those electrons which have emitted a $\langle 111\rangle$ phonon. As a result, $\Delta R/R$ should decrease when ΔE increases. This trend is observed in Fig. 22.

VI. CONCLUSION

We have demonstrated that tunneling in Schottky barriers under hydrostatic pressure is in two respects a powerful and promising technique. First, band-structure effects can be used to study the tunneling mechanism and its spectroscopic nature. We have confirmed that a pure specular process together with some simplifications of the model (no band tailing, parabolic barrier shape, WKBJ approximation) conveniently describes the background resistance curve, even when the central band is nearly depleted of electrons. Our results further elucidate the zone-boundary phonon tunneling process and some puzzling features of the electron-plasmon [LO(000)-phonon] interaction. Further quantitative interpretation of these results is presently under study.

A second aspect of tunneling under pressure is that in some cases it can aid in the investigation of semiconductor band structure. The tunnel current is so sensitive to some parameters that the comparison between theory and experiment is affected substantially by the use of wrong values for m^*, V_B, or ΔE. For example, R_0 is multiplied by 2.5 when m^* increases by 12%. Furthermore, the shape of dV/dI is so dependent on ΔE that band crossing gives rise to effects much larger than those which occur in a semiconductor like GaAs[17] in the same pressure range. Therefore, a fit between theory and experiment can be considered as a good means for determining some important parameters in a given material. From our results, we can estimate the limits of ΔE. In the indirect-gap configuration, the zone-boundary-assisted processes become very weak when $|E_L-E_\Gamma|>300$ meV.[44] Moreover, at reverse bias, it is difficult to apply voltages higher than 300 mV to observe the onset of tunneling into the central band. In the direct-gap configuration, the heavy mass valleys can be detected only if they are filled with carriers and therefore have an influence on the value of the Fermi degeneracy. This occurs for GaSb at room pressure but this was not the case for GaAs even at 17 kbar.[45] Briefly, the condition for two bands to be detected can be written approxi-

mately as

$$-300 \text{ meV} < \Delta E < 100 \text{ meV} , \quad (8)$$

where $E = E_L - E_\Gamma$ or $E_X - E_\Gamma$. *A priori*, it seems that such an experiment could provide significant data on the band structure of III-V compounds. Unfortunately, InSb experiences a phase transition at 22 kbar[46] before condition (8) can be verified, and GaP, AlSb, AlAs show values of $E_X - E_\Gamma$ lower than -500 meV at any pressure. GaAs seems more favorable if the applied pressure can reach 30 kbar. On the other hand, III-V ternary compounds may offer an interesting field of investigation, especially GaAlAs, GaInP, and GaAsP, at compositions which correspond to the crossing of the Γ and X bands. The main drawback of these materials is that their large energy gaps lead to high values of V_B. Moreover, the effective masses in the X valleys are very high. As a consequence the compounds must be heavily doped, which is not always possible.

In summary, band-structure effects in Schottky barriers under pressure manifest themselves as huge changes of the first-derivative plots. The reliability of such structures is better than that of other tunnel junctions; the barrier is a property of the contact itself, the interface can be nearly free from impurities and the theory is in fairly good agreement with the experiment. All these features give us confidence to recommend using the method for the measurement of interband energy gaps, zone-boundary-phonon energies, Grüneisen parameters, effective masses, and superconducting parameters under pressure.

ACKNOWLEDGMENTS

We wish to thank D. Jerome for making available the high-pressure apparatus of Orsay and Professor E. Guyon for his constant interest in this work. We are grateful for the comments of Professor M. P. Shaw (Wayne State University, Michigan) regarding the preparation of the manuscript. R. Duchesne and M. Nelson-Pauthier are acknowledged for their skillful technical help.

APPENDIX A: HALL EFFECT

The relations between N, μ_F, and R_H, the Hall coefficient, are expressed by

$$N = N_0 + N_1 = \frac{4\pi}{h^3} (2m_0^* kT)^{3/2} \left[F_{1/2}\left(\frac{\mu_F(000)}{kT}\right) + 4\left(\frac{m_{1d}^*}{m_0^*}\right)^{3/2} F_{1/2}\left(\frac{\mu_F(000) - \Delta E}{kT}\right)\right] , \quad (A1)$$

which can be written at 4.2 °K as

$$N = \frac{8\pi}{3h^3} (2m_0^*)^{3/2} \left[\mu_F^{3/2}(000) + 4\left(\frac{m_{1d}^*}{m_0^*} (\mu_F(000) - \Delta E)\right)^{3/2} \right] , \quad (A2)$$

and

$$R_H = \frac{r_0}{N_0 e} \left[1 + \frac{N_1}{N_0}\left(\frac{\mu_1}{\mu_0}\right)^2 F \right] \Big/ \left(1 + \frac{N_1}{N_0} \frac{\mu_1}{\mu_0}\right)^2 , \quad (A3)$$

where

$$F = 3K(K+2)/(2K+1)^2 . \quad (A4)$$

N_0 and N_1 are the carrier densities in the $\Gamma\langle 000 \rangle$ band and the $L\langle 111 \rangle$ valleys, respectively. At low temperature, if $R_H > 5$ cm^3/C, R_H reduces to r_0/Ne.[8] Calculations were performed with the parameters listed in Table II. Fermi integrals and r_0 values were taken from Ref. 47. The result of the calculation is shown in Fig. 26 and was used to deduce N from the Hall measurements. Results seem consistent, although in some samples the N values are slightly lower at 300 than at 77 °K (~ 10%). Uncertainties in the parameters are responsible for this anomaly.

APPENDIX B: BAND-CROSSING ANOMALY

We shall demonstrate in this Appendix that the resistance anomaly reported in Sec. IV D can be explained by the reflection of the superconducting density of states of the lead at the sharp resistance increase which occurs between $V=0$ and $eV = \mu_F(000)$. The tunnel current at 0 °K in a Schottky barrier with the metal in the normal state can be written

$$I = \frac{2eA\rho_\parallel}{h} \int_a^{\mu_F} dE \int_0^E dE_\parallel D(eV;\, E - E_\parallel) , \quad (B1)$$

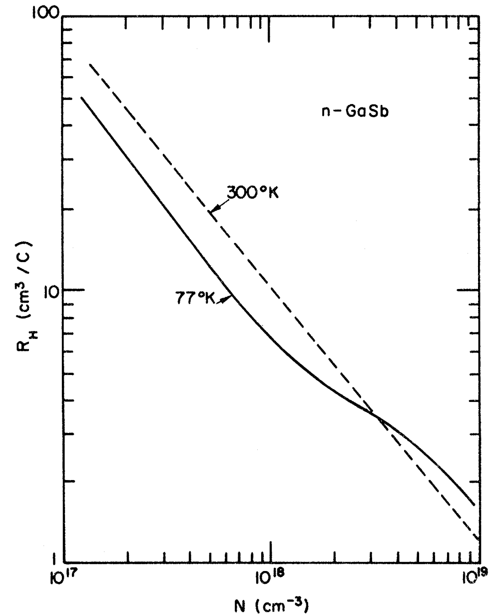

FIG. 26. Hall coefficient vs carrier density at 300 and 77 °K in n GaSb.

with

$$a=\begin{cases}\mu_F - eV & \text{for } eV < \mu_F\\ 0 & \text{for } eV \geq \mu_F\ .\end{cases}$$

V is the applied voltage, μ_F is the Fermi degeneracy measured from the band edge. E and $E_\parallel$ are, respectively, the total energy and the kinetic energy related to the motion parallel to the junction plane, both measured from the bottom of the conduction band. A is the contact area and

$$\rho_\parallel = m^*/2\pi h^2\ . \tag{B2}$$

m^* is the effective mass in the parabolic conduction band, D is the transmission coefficient, and e is the absolute value of the electron charge.

Consider the situation in which the *positive* bias V is smaller than μ_F/e. When the metal is in the normal state, Duke calculated the shape of the conductance as a function of V.[48] D may be approximated by a constant D_0.[49] We obtain

$$I \approx \frac{2eA\rho_\parallel D_0}{h}\int_a^{\mu_F} E\, dE \tag{B3}$$

and

$$G=\frac{dI}{dV}\approx\frac{2e^2A\rho_\parallel D_0}{h}\,(\mu_F - eV)\,\theta(\mu_F - eV)\ . \tag{B4}$$

The linear variation of G is illustrated in Fig. 27 (dotted line). The same approximate model is now applied to the case of a superconducting metal

$$I \approx \frac{2eA\rho_\parallel D_0}{h}\int_b^{\mu_F} EN_S(eV+E-\mu_F)\, dE\ , \tag{B5}$$

with

$$b=\begin{cases}\mu_F - eV+\Delta & \text{for } eV < \mu_F+\Delta\\ 0 & \text{for } eV \geq \mu_F+\Delta\ .\end{cases}$$

N_S, the superconducting density-of-states factor, is given by

$$N_S(x)=\begin{cases}x/(x^2-\Delta^2)^{1/2}\ , & |x|>\Delta\\ 0\ , & |x|<\Delta\ .\end{cases} \tag{B6}$$

Changing variables,

$$I \approx \frac{2eA\rho_\parallel D_0}{h}\int_c^{eV} (x+\mu_F - eV)\, N_S(x)\, dx\ , \tag{B7}$$

with

$$c=\begin{cases}\Delta & \text{for } eV < \mu_F+\Delta\\ eV-\mu_F & \text{for } eV \geq \mu_F+\Delta\ .\end{cases}$$

The derivative of the integral J leads to

$$\frac{dJ}{dV}=\theta(\mu_F+\Delta-eV)\left(\mu_F N_S(eV)-\int_\Delta^{eV} N_S(x)\,dx\right) + \theta(eV-\mu_F-\Delta)\left(\mu_F N_S(eV)-\int_{eV-\mu_F}^{eV} N_S(x)\,dx\right). \tag{B8}$$

Then

$$G\approx\frac{2e^2A\rho_\parallel D_0}{h}\left(\mu_F N_S(eV)-\int_\Delta^{eV} N_S(x)\,dx + \theta(eV-\Delta-\mu_F)\int_\Delta^{eV-\mu_F} N_S(x)\,dx\right), \tag{B9}$$

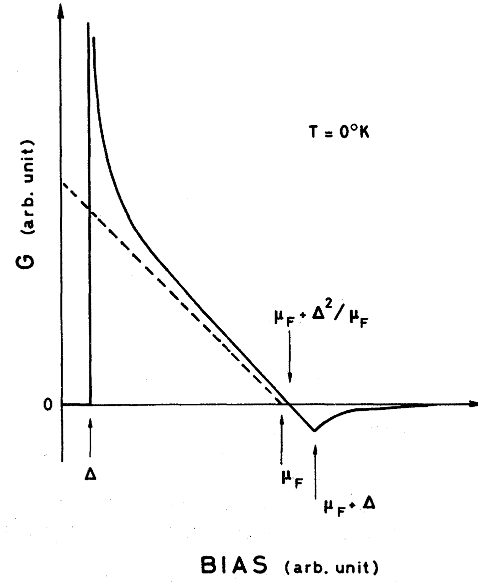

FIG. 27. Schematic drawing explaining the origin of the band-crossing anomaly (see Appendix B).

that is,

$$G\approx\frac{2e^2A\rho_\parallel D_0}{h}\{\mu_F N_S(eV)-[(eV)^2-\Delta^2]^{1/2} + \theta(eV-\Delta-\mu_F)[(eV-\mu_F)^2-\Delta^2]^{1/2}\}\ . \tag{B10}$$

At low bias the first two terms illustrate the appearance of the superconducting density of states on the first-derivative curve. The voltage at which $G=0$ is calculated from

$$\mu_F N_S(eV)=[(eV)^2-\Delta^2]^{1/2}\ . \tag{B11}$$

(B6) and (B11) lead to

$$G=0 \quad \text{for } eV=\mu_F+\Delta^2/\mu_F \ (\text{when } 4\Delta^2<\mu_F^2)\ . \tag{B12}$$

When $eV\geq\mu_F+\Delta$ the contribution of the second and third terms of (B10) lead to an undershoot on the G-vs-V curve (Fig. 27, full line). At higher bias Δ can be neglected, $N_S=1$, and $G\to 0$. In summary, the *discontinuity* of the conductance at $eV\simeq\mu_F$ is modulated by the superconducting density of states. This appears in much the same way as the reflection of this density of states on the conductance structures induced by inelastic processes. In the actual case D is not perfectly constant between 0 and $eV=\mu_F$; it seems more realistic that G does not decrease to zero. Even in this case the differential resistance $R=1/G$ may experience a strong peak at $\mu_F+\Delta$. Our experiments at 11 kbar (Fig. 9) have shown that $R(\mu_F)/R(0)$ can be equal to 20. Thus, it is not surprising that such a strong change of R (i.e., of G) leads to the appearance of a sharp resistance peak (Fig. 15).

*Work supported by the Délégation Générale à la Recherche Scientifique et Technique.

†Work constitutes the main part of a Doctorat d'Etat ès Sciences Physiques presented at the Faculté des Sciences d'Orsay, June 1972.

[1]C. B. Duke, *Tunneling in Solids* (Academic, New York, 1969).

[2]*Tunneling Phenomena in Solids*, edited by E. Burstein and S. Lundqvist (Plenum, New York, 1969).

[3]J. W. Conley and J. J. Tiemann, J. Appl. Phys. 38, 2880 (1967).

[4]F. Steinrisser, L. C. Davis, and C. B. Duke, Phys. Rev. 176, 912 (1968).

[5]L. C. Davis and F. Steinrisser, Phys. Rev. B 1, 614 (1970).

[6]P. Guétin and G. Schréder, Phys. Rev. Letters 27, 326 (1971).

[7]A. Sagar, Phys. Rev. 117, 93 (1960).

[8]W. M. Becker, A. K. Ramdas, and H. Y. Fan, J. Appl. Phys. 32, 2094 (1961).

[9]G. D. Pitt, High Temp. High Pressure 1, 118 (1969).

[10]R. W. Keyes and M. Pollak, Phys. Rev. 118, 1001 (1960).

[11]A. L. Edwards and H. G. Drickamer, Phys. Rev. 122, 1149 (1961).

[12]E. H. van Tongerloo and J. C. Wooley, Can. J. Phys. 47, 241 (1969).

[13]M. Cardona, J. Phys. Chem. Solids 17, 336 (1961).

[14]B. M. Vul, E. I. Zavaritskaya, and S. D. Denisov, Fiz. i Tekh. Poluprovodnikov 3, 1961 (1969) [Sov. Phys. Semicond. 3, 1421 (1970)].

[15]T. O. Yep and W. M. Becker, Phys. Rev. 156, 939 (1967).

[16]D. G. Seiler and W. M. Becker, Phys. Rev. 186, 784 (1969).

[17]P. Guétin and G. Schréder, Phys. Rev. B 5, 3979 (1972).

[18]G. Malfait and D. Jerome, Rev. Phys. Appl. 4, 467 (1969).

[19]D. E. Thomas and J. M. Rowell, Rev. Sci. Instr. 36, 1301 (1965).

[20]A. M. Goodman and D. M. Perkins, J. Appl. Phys. 35, 3351 (1964).

[21]A. M. Goodman, J. Appl. Phys. 34, 329 (1963).

[22]C. A. Mead and W. G. Spitzer, Phys. Rev. 134, A713 (1964).

[23]P. Guétin and G. Schréder, J. Appl. Phys. 42, 5689 (1971).

[24]J. W. Conley and G. D. Mahan, Phys. Rev. 161, 681 (1967).

[25]D. C. Tsui, Phys. Rev. Letters 22, 293 (1969).

[26]C. B. Duke, M. J. Rice, and F. Steinrisser, Phys. Rev. 181, 733 (1969).

[27]K. L. Ngai, E. N. Economou, and M. H. Cohen, Phys. Rev. Letters 22, 1375 (1969).

[28]C. B. Duke, Phys. Rev. 186, 588 (1969).

[29]D. C. Tsui and A. S. Barker, Phys. Rev. 186, 590 (1969).

[30]E. N. Economou and K. L. Ngai, Phys. Rev. B 4, 4105 (1971).

[31]M. Mikkor and W. C. Vassell, Phys. Rev. B 2, 1875 (1970).

[32]M. Hass and B. N. Henvis, J. Phys. Chem. Solids 23, 1099 (1962).

[33]P. Guétin and G. Schréder, J. Appl. Phys. 43, 549 (1972).

[34]A slight ion bombardment leads to an additional structure, even in conductance, which appears just at the onset of the line shape of the LO(000) structure. Its origin is unclear at the present time.

[35]B. B. Kosicki, Harvard University Division of Engineering and Applied Physics Technical Report No. HP-19, 1967 (unpublished).

[36]J. V. Morgan and E. O. Kane, Phys. Rev. Letters 3, 466 (1959).

[37]N. Holonyak, Jr., I. A. Lesk, R. N. Hall, J. J. Tiemann, and H. Ehrenreich, Phys. Rev. Letters 3, 167 (1959).

[38]L. Esaki and Y. Miyahara, Solid State Electron. 1, 13 (1960).

[39]D. E. Cullen, E. L. Wolf, and Dale Compton, Phys. Rev. B 2, 3157 (1970).

[40]R. T. Payne, Phys. Rev. 139, A570 (1965).

[41]H. Fritzsche and J. J. Tiemann, Phys. Rev. 130, 617 (1963).

[42]G. Schréder, Doctorate thesis (University of Paris, 1972) (unpublished).

[43]G. A. Slack and S. Roberts, Phys. Rev. B 3, 2613 (1971).

[44]P. Guétin and G. Schréder (unpublished).

[45]P. Guétin and G. Schréder, Solid State Commun. 9, 591 (1971).

[46]J. C. Jamieson, Science 139, 845 (1963).

[47]V. E. Fistul, *Heavily Doped Semiconductors* (Plenum, New York, 1969).

[48]C. B. Duke, Ref. 2, p. 40.

[49]The validity of the WKBJ approximation at the band edge is questionable because the wavelength of electrons is very large. However, we have shown along this article that the WKBJ approximation takes into account the most part of the experimental results at any pressure.